2010 IEEE International Conference on Robotics and Automation
Anchorage Convention District
May 3-8, 2010, Anchorage, Alaska, USA

# Design and Control of a Novel 3D Casting Manipulator

Adriano Fagiolini, Felipe A. W. Belo, Manuel G. Catalano,
Fabio Bonomo, Simone Alicino, and Antonio Bicchi

*Abstract*— **This paper focuses on casting manipulation and presents an innovative mechanism that allows objects placed in a three–dimensional space to be reached with a relatively small robot. Casting manipulation is a technique by which a robotic end–effector is thrown and its ballistic flight is controlled through a tether cable so as to reach a target object. Previous work presented a solution that is viable only when the position of the target object is perfectly known or aligned with the throwing plane. Our work extends the technique by use of a novel mechanical design of the arm, and a suitable control scheme for the flight of the end–effector, which makes it applicable for objects placed at generic positions in a three–dimensional environment. Effectiveness of the casting robot was shown during the first ESA Lunar Robotics Challenge, where our team came in the second place.**

## I. Introduction

In several robotic applications, such as planetary explorations or rescue missions in devastated areas, velocity of task execution must be traded for robustness to asperities of unstructured terrains, or debris–strewn lands. To regain task performance within such scenarios, a large workspace would afford a great potential advantage. However, to operate on objects at distances several times larger than the physical dimensions of the robot, mobile platforms [1] equipped with articulated arms are practically the only available solution at the state of the art. Notwithstanding, wheeled or legged robotic locomotion depends heavily on the characteristics of the terrain. In fact, e.g., Martian explorers Spirit and Opportunity traveled at max. 180 m/h speed, on an average mission length of 100 meters from the base station, thus limiting the number of samples returned per day. On the other hand, the alternative of building arms with either very long links [2] or many links [3], [4] seems to be applicable only in some very specific cases, for instance in the absence of gravity, and yet imposes the use of very wide mechanical structures despite the extension of their reachable spaces.

Among these applications, planetary exploration missions involving material sample acquisition and return pose special challenges due to the fact that any kind of human intervention is impossible during the mission itself. In this context, during October 2008, the European Space Agency (ESA) carried out the first Lunar Robotics Challenge (LRC) [5], in which we participated, to motivate and accelerate research and development of tele–operated rovers. The short–term objective of the very competitive challenge was the realization of a robotic vehicle capable of retrieving soil samples through remote operation from a lunar crater located at South Pole of the Moon. For that reason, the challenge was held at the Minas de San José in the National Park of Teide on Tenerife Island, whose roughness and surface texture is similar to that of the crater on the Moon. The Challenge, and indeed the real mission that is being simulated by it, poses the further risk of loosing the rover down in the dark crater, if some error occurs and thus the rover cannot recharge its batteries.

Authors are with the Interdepartmental Research Center "E. Piaggio" of the Università di Pisa, Italy; Email: {a.fagiolini, felipe.belo, bicchi}@ing.unipi.it, {manuel.catalano, fabio.bonomo }@gmail.com, simone.alicino@fastwebnet.it.

Fig. 1. DAVID, the University of Pisa's rover for the first ESA Lunar Robotics Challenge, in a suggestive scene of Mount Teide in Tenerife Island.

To reduce the distance to be traveled on the difficult terrain and avoid risks in reaching the lowest and sunless parts of the crater, we proposed the use of a vehicle (see Fig. 1) that was endowed with a casting manipulator, i.e. an arm that allows a robotic end–effector to be deployed at large distance from the robot's base by throwing it and controlling its ballistic flight through a tether cable so as to reach a far target position. Operation phases of the casting mechanism comprise a *startup phase*, a *steering phase*, and a *retrieval phase*. During the startup phase, the robot is controlled so as to impart the end–effector sufficient mechanical energy to reach the target object. When the first phase concludes, the end–effector is thrown, and its trajectory is steered by means of forces transmitted through the tether cable in order to approach the object with suitable orientation and velocity (steering phase). Once the object has been caught, the tether cable is reeled up and the object is retrieved (object–return phase).

978-1-4244-5040-4/10/$26.00 ©2010 IEEE

Casting manipulation was originally proposed by Arisumi *et al.* in [6]. Therein, the ability of a simple casting robot, composed of a swinging arm and a gripper, to fetch distant objects placed at *a priori* known positions on the throwing plane was demonstrated with early hardware prototypes. The gripper's landing position, orientation, and velocity were controlled by transmission of 3 short–duration forces (up to 50 msec) through the tether cable. The gripper's orientation and residual kinematic energy were chosen so as to allow grasping of a spherical object. A–priori knowledge of the target position was necessary since computation of impulsive forces' times and durations cannot be afforded online. The technique was extended to moving objects or objects placed at a priori uncertain positions in [7], by closing a real– time visual feedback loop of the target object on the casting manipulation. To cope with a moving object, a simpler dynamic model of the end–effector's flight was presented, that allows real–time computation of the force to be transmitted through the tether cable.

The main limitation of these early casting robots is the requirement that the target position lay on the throwing plane. However, even if the end–effector's flying plane is initially aligned with the direction of the target, inherent uncertainty in the model or in the actuation and external disturbances, due to e.g. the wind, will eventually mislead the end–effector itself. This fact motivates our research in developing a casting manipulator that is able to steer a robotic end–effector in a three–dimensional space. A preliminar analysis of the performance of such a casting robot was performed through simulation in [8], whereas the final prototype that was actually used during the Challenge is described in [9]. Therein, a simplified model for the end–effector's flight that is valid only when the casting manipulator main arm is in the upright position was presented. In this paper, a general and more accurate dynamic model is presented along with a suitable control of the robot. Moreover, the paper describes a planning scheme for the trajectory of the end–effector that allows a generic position in a 3–dimensional space to be reached.

The paper is organized as follows. Section II describes the novel design of a casting arm. Section III describes the arm's kinematics and the dynamics of the end–effector during the flight phase. Following section IV presents the proposed scheme for planning the trajectory of the end–effector. Section V describes the hardware setup of the casting mechanism that was used during the Challenge and reports the results and performance evaluation of the robot. Final Section VI summarizes the work achievement and describes relevant future development.

## II. Mechanical Design of the 3D Casting Manipulator

Consider the casting manipulator reported in Fig. 2, whose mechanical structure is described in the following. The first link is composed of two plates and a hub (No 1 in the figure) housing the robot's shaft (2), and it is actuated by a servomotor (7). The link is connected to the rover's base platform through a revolute joint $\theta$ that is referred to as tilt. Then, a second revolute joint $\alpha$ connects a rigid arm (3) that represents the robot's second link. To reduce undesired vibrations due to a high–speed rotation of the second link, a counterbalancing bar (4) is hinged to the link that allows installation of an interchangeable weight (5). A second servomotor (6) is placed at the second link's base and is connected to the robot's shaft through a gear box $(12-13)$ which provides a gear ratio of 3. A tether cable (14) is used to connect a robotic end–effector to the robot's base. A series of pulleys (see e.g. No 15) is installed along the second link to allow the tether cable running with reduced friction inside the shaft. The cable is initially winded around a reel (10) that is integral with the rotor of an electromagnetic clutch (9). The stator of the clutch is instead attached with a third servomotor (8). Three optical encoders are embedded into the servomotors' controllers and one (11) is used to measure the length $\rho$ of the tether cable. A plate (16) forms the platform of the rover and the base of the casting mechanism.

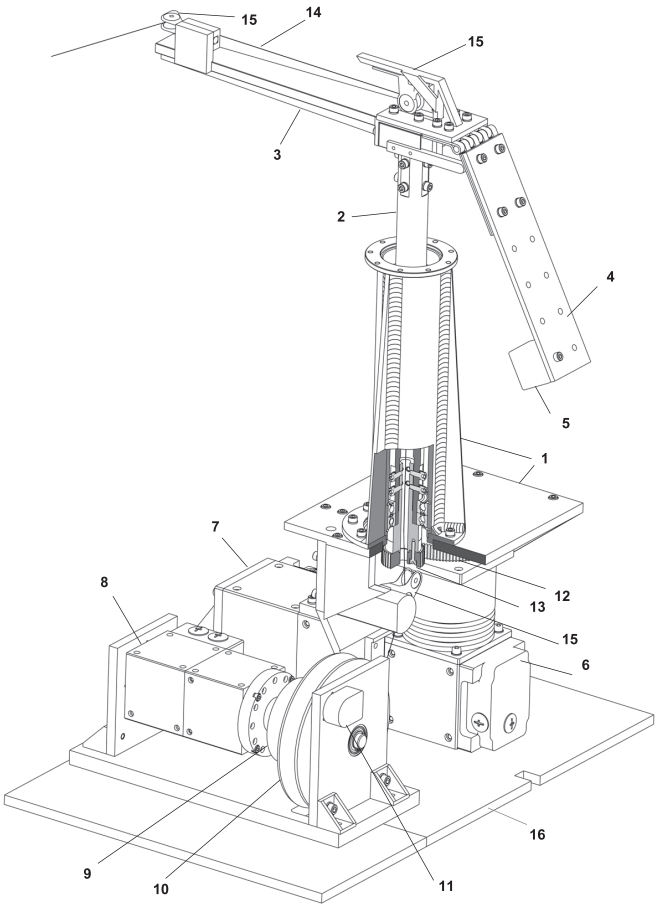


Fig. 2. View of the 3D casting manipulator with detail of its components (1. hub, 2. hollow shaft, 3. arm, 4 counterbalancing bar, 5. counterweight, 6. second link's motor, 7. tilt motor, 8. reel's motor, 9. electromagnetic clutch, 10. reel, 11. optical encoder, 12. driving gear, 13. driven gear, 14. cable, 15. pulleys, 16. rover's platform).

The design of the casting manipulator has addressed issues

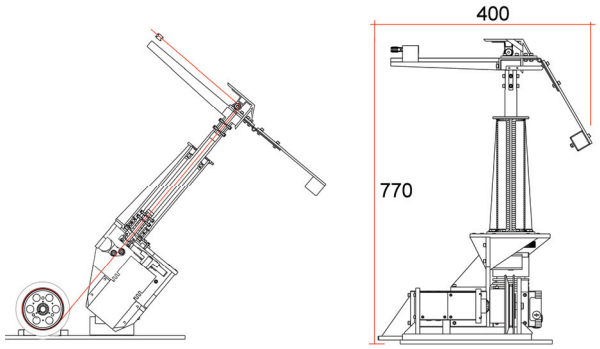


Fig. 3. Side view of the casting manipulator with the tether cable highlighted in red (left), and occupancy in millimeters of the robot when deployed in the upright rest position (right).

related to structural analysis, such as weight, volume and vibrations. Most of its composing elements are made of aluminum alloy, that provides high fatigue resistance despite of it lightness. The manipulator guarantees low volume occupancy when stowed ($\theta = 0$ rad), as it was required by the Challenge's specifications. The dimensions of the links (as well as the initial length of the cable) have been chosen so that any collision between the casting mechanism and the end–effector or the arm itself is prevented. Fig. 3–(right) shows the casting mechanism's dimensions when it is unpacked. Choice of the first servomotor, actuating $\theta$, has taken into account all loads that have to be supported during the startup and steering phases.

Furthermore, as it is well–known, the use of cables poses various other problems in the application. Some of them are listed in the following:

- ▷ *Cable twisting due to axial rotation of the shaft*: Problems due to the twisting are limited with a cable with a smaller diameter, which on the contrary offers less resistance to centrifugal forces. Experience shows that the effect of twisting can be neglected for cable with diameter in $[0.1, 0.5]$ mm. Among available commercial solutions, a polyethylene–fiber rope, called Dyneema, with a diameter of $0.2$ mm have been chosen as it offers sufficient resistance to loads.
- ▷ *Cable entanglement due to instantaneous landing of the end–effector*: After the end–effector's landing, the cable is prone to wrap around the reel. To avoid this, active control of the reel by means of the actuator mounted on the clutch must reduce or stop the cable unwinding after the end–effector's landing.
- ▷ *Cable misalignment and nesting inside the shaft*: Pulleys are used to prevent nesting of the cable (other than reducing viscous friction only). The path of the cable, highlighted in red in Fig. 3–(left), has been optimized for the optimal tilt angle, i.e. the angle allowing longer throwing range.

## III. Modeling and Control

Due to the presence of a flexible part, modeling of a casting manipulator may represent a complex task. In fact,

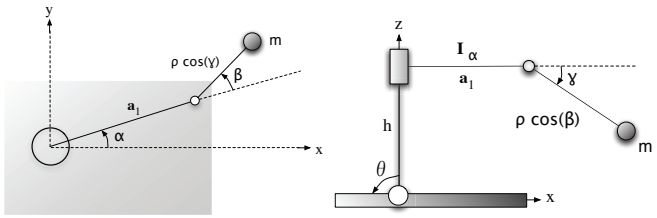


Fig. 4. Generic configuration of the casting manipulator: top view (left) and side view (right).

a sufficiently accurate description of its dynamic behavior in a generic operation mode can be obtained through use of finite–element methods, as it was shown in [10], but this is possible at the expense of high computation demands. On the contrary, a simplified yet accurate model of the startup and steering phases can be obtained by assuming that the adopted control strategy guarantees that the tether never becomes loose and that elastic modes are not excited [6]. Under this hypothesis, the behavior of the tether cable can be approximated as that of a rigid link.

Referring to Fig. 4, let us denote with $q = (\alpha, \rho, \gamma, \beta)^T$ the robot's configuration, and with $\theta$ a constant tilt angle. Then, the position $p = (x, y, z)^T$ of the end–effector can be computed by the direct kinematics

$$p = k(q)$$

that is reported in the appendix. By differentiating w.r.t. time, it is straightforward to obtain the differential kinematics

$$\dot{p} = J(q)\,\dot{q}$$

that expresses the end–effector's velocity based on the knowledge of the joints' configuration and velocity (see again the appendix for explicit terms). Moreover, having denoted with $\tau_\alpha$ and $f$ the torque and force applied by motors at the joints represented by $\alpha$ and $\rho$, respectively, the robot's dynamics can be conveniently written in the classical form

$$\mathrm{B}(q)\,\ddot{q} + h(q, \dot{q}) = \tau\,, \tag{1}$$

where $\tau = (\tau_\alpha, -f - c_\rho\,\dot{\rho}, -c_\gamma\,\dot{\gamma}, -c_\beta\,\dot{\beta})^T$ is the generalized force vector, $c_\rho, c_\gamma, c_\beta \geq 0$ are friction coefficients, and $h = (h_\alpha, h_\rho, h_\gamma, h_\gamma)^T$. Explicit values of the dynamics are reported in the appendix. It is worth noting that the tether cable can exert only a pulling force on the end–effector, i.e. $f \geq 0$.

A control scheme for the casting manipulator can be derived as follows. Left–multiply Eq. 1 by the inertia matrix inverse, $\mathrm{B}(q)^{-1} = \{\tilde{b}_{ij}\}$, thus obtaining

$$\ddot{q} = \mathrm{B}(q)^{-1}\,(\tau - h(q, \dot{q}))\,,$$

whose first row reads

$$\begin{aligned} \ddot{\alpha} &= \tilde{b}_{11}(q)\,(\tau_\alpha - h_\alpha(q, \dot{q})) + \tilde{b}_{12}(q)\,(f - h_\beta(q, \dot{q})) + \\ &- \tilde{b}_{13}(q)\,h_\gamma(q, \dot{q}) - \tilde{b}_{14}(q)\,h_\beta(q, \dot{q}) = \\ &= \tilde{b}_{11}(q)\,\tau_\alpha - \eta_\alpha(q, \dot{q}, f)\,. \end{aligned}$$

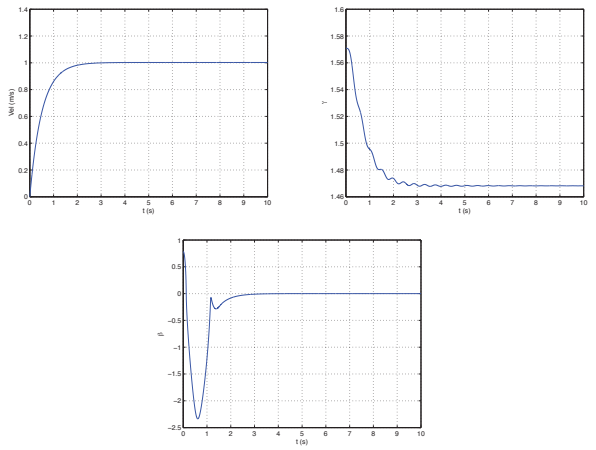

Fig. 5. Results from simulation of a startup phase with initial configuration values $\alpha(0) = 0$ rad, $\rho(0) = 1$ m, $\gamma(0) = \pi/2$ rad, and $\beta(0) = 0$, and final velocity $\dot{\alpha} = 1$ rad/s.

Then, given a desired trajectory $\bar{\alpha}(t)$, the nonlinear feedback law

$$\bar{\tau}_\alpha = \frac{1}{\bar{b}_{11}(q)} \left(\eta_\alpha(q, \dot{q}, f) + \ddot{\bar{\alpha}} + k_v(\dot{\alpha} - \dot{\bar{\alpha}}) + k_p(\alpha - \bar{\alpha})\right)$$

with $k_p, k_v > 0$, yields

$$\begin{pmatrix} \ddot{\alpha} \\ \ddot{\rho} \\ \ddot{\gamma} \\ \ddot{\beta} \end{pmatrix} = \begin{pmatrix} \ddot{\bar{\alpha}} + k_v(\dot{\alpha} - \dot{\bar{\alpha}}) + k_p(\alpha - \bar{\alpha}) \\ \Psi_\rho(q, \dot{q}, \bar{\alpha}, \dot{\bar{\alpha}}, f) \\ \Psi_\gamma(q, \dot{q}, \bar{\alpha}, \dot{\bar{\alpha}}, f) \\ \Psi_\beta(q, \dot{q}, \bar{\alpha}, \dot{\bar{\alpha}}, f) \end{pmatrix},$$

where the first joint variable $\alpha$ is stabilized. The system can then be conveniently written as

$$\ddot{q}(t) = \Psi(q(t), \dot{q}(t), \bar{\alpha}(t), \dot{\bar{\alpha}}(t), f(t)) \,. \tag{2}$$

The robot's dynamic model and the above derived control are valid as long as the tether cable's looseness is prevented. To this aim, the rotation $\alpha(t)$ is chosen s.t. the centrifugal force acting on the end–effector always pulls the tether cable. Fig. 5 reports the simulation of a startup phase with initial configuration values $\alpha(0) = 0$ rad, $\rho(0) = 1$ m, $\gamma(0) = \pi/2$ rad, and $\beta(0) = 0$, and final velocity $\dot{\alpha} = 1$ rad/s.

## IV. Steering Phase Trajectory Planning

The casting manipulation problem basically consists of throwing a robotic end–effector and controlling its ballistic flight through use of the tether cable. Therefore, it is quite natural to split the steering problem into the sequence of problems

*Problem 1 (Trajectory planning):* Based on a–priori knowledge of the target position $p_t = (x_t, y_t, z_t)^T$, find a suitable throwing state $x = (p(0), \dot{p}(0))^T$ of the end–effector s.t. it can reach $p_t$ after a flight time $t_f$.

*Problem 2 (Feedback control):* Given the current target position $p_t(t)$ and the current end–effector's state $x$, find feedback control laws $\tau_\alpha(x, p_t)$ and $f(x, p_t)$ s.t. the end–effector can reach the target position.

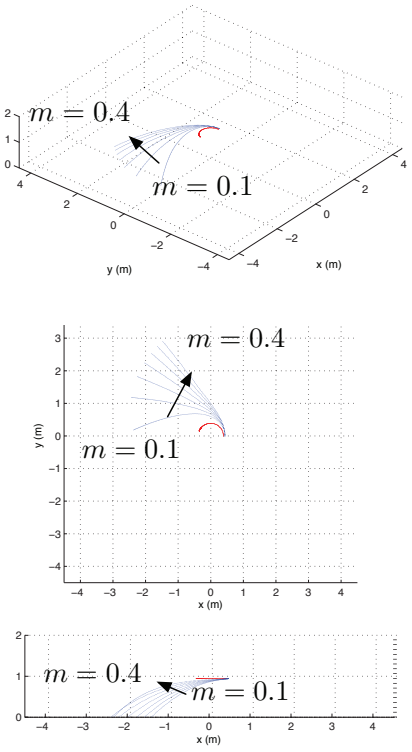


Fig. 6. Results from simulation of steering phase with same throwing configurations ($\dot{\alpha} = 1$ rad/s), but different masses.

Feedback control of the end–effector via use of the tether cable's force is an open problem that will deal with in future work. This work focuses on Problem 1 that can be solved by finding solution to the optimization problem

$$\begin{cases} (\bar{q}(0), \dot{\bar{q}}(0)) = \arg\min \left(||p(t_f) - p_t||^2\right) \,, \\ p(t) = k(q(t)) \,, \\ \ddot{q}(t) = \Psi(q(t), \dot{q}(t), \bar{\alpha}, \dot{\bar{\alpha}}, f(t)) \,, \\ f = 0 \,, \\ q(0) = \bar{q}(0) \,, \; \dot{q}(0) = \dot{\bar{q}}(0) \,, \\ t_f \geq 0 \,. \end{cases} \tag{3}$$

The robot's controlled dynamics $\Psi$ is valid also during the steering phase, if again the tether cable is controlled so that its looseness is prevented. This can easily be achieved by gradually decreasing $\alpha(t)$ after the throwing. The angle $\alpha$ is also chosen so that the first link approximately follows the end–effector's flight direction, which reduces friction at the last pulley (No 15 in Fig. 2). Due to the nonlinearity of the robot's dynamics $\Psi$, it is not possible to find an analytical solution of Problem 3, which can only be sought via numerical integration of $\Psi$ itself and the use of iterative methods for parameter optimization based on gradient–descent. Fig. 6 and Fig. 7 show 3D trajectories of an end–effector with different masses and different tilt angles conditions, respectively.

## V. Experimental Setup and Results

The experimental prototype, that was also used during the Challenge, consists of a rover (see Fig. 1) equipped

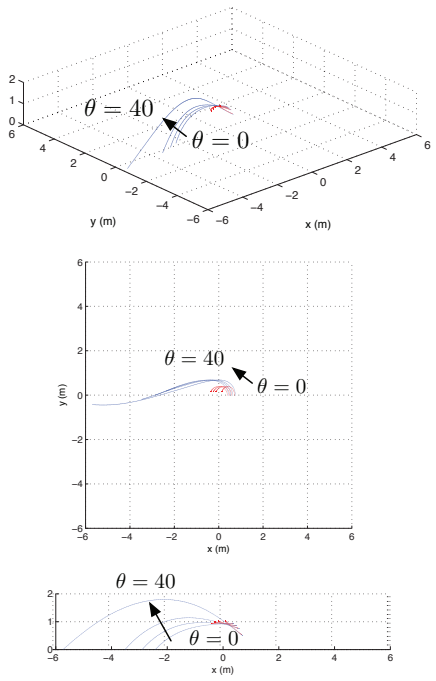


Fig. 7. Results from simulation of a steering phase with same throwing configurations ($\dot{\alpha} = 1$ rad/s), but different tilt angle $\theta$.

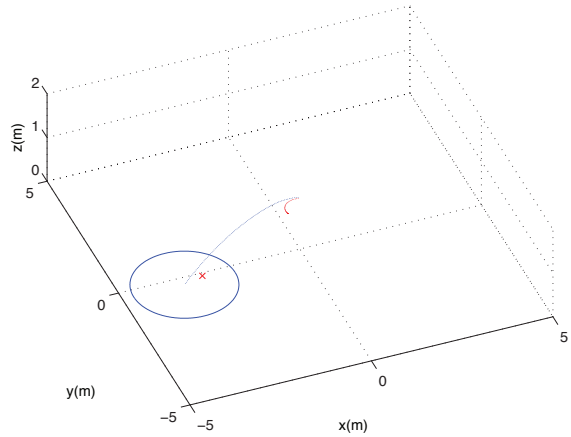


Fig. 8. Steering phase experiment (the red line is the second arm trajectory, the blue line is the end–efffector's simulated trajectory, the red cross is the final experimental position, and the circle is the region of expected landing.

with a casting manipulator. The robot has an embedded controller that has been developed in LabVIEW 8.6, runs over a National Instrument CompactRIO (cRIO-9014), and uses a Compact Vision System (CVS). Various modules have been implemented: analog and digital I/O, two CANBus ports, eight RS232 ports, and some relays. Actuation of the casting mechanism consists of a Schunk PR90 motor for the joint $\theta$, a Schunk PDU90 motor connected to the gearbox to actuate the joint $\alpha$, and a Schunk PR70 motor for the reel (joint variable $\rho$). For in–lab experiments, a mass of $m = 388$ g was used as the end–effector. A vision system composed of Imaging Source DFK21AF04-Z color camera with mechanical zoom and two DBK24AF04 color cameras were mounted on the rover during the Challenge. An Acuity Research PTU-46 pan-tilt was also used. For measuring the end–effector's landing position, an Acuity Laser Measurement AR1000 laser was used.

The effectiveness of the casting mechanism has been shown in experiments reported in [9]. A comparison between experimental and simulation results of the steering phases is reported in Fig. 8. The experimental results corresponded to expectations based on the simulated model only partially. This is due in part to the inaccuracies in estimating some of the model parameters, in part to non–modeled effects that are present e.g. at the electromagnetic clutch, and in part to hardware limits that impose lower bounds to e.g. the scheduling period of the control process. Uncertain parameters can be collected in a vector $\lambda = (I_r, I_b, m, k_s, k_p, \alpha(0), \rho(0))^T$, whose components represent the reel inertia, the first link length, the end-effector's mass, motors' saturation and proportional constant, and the throwing configuration. The end–effector's dynamics can be rewritten in the form

$$\dot{x} = \Psi(x, \lambda, u),$$

with $u = (\tau, f)$, and thus its solution at the generic time $t$ can be described as $x(t) = \phi_\Psi(\lambda, u, t)$. Assuming a variation $\delta\lambda$ of the uncertain parameters from the nominal value $\lambda$ and a maximum variation $\delta u$ in the control, the corresponding variation in the end–effector's state at time $t$ can be approximated by the first–order expansion of the system's solution. Then, the maximum expected errors in the end–effector's position is

$$||\delta p(t)|| \leq \left|\left| \frac{\partial \phi_\Psi(\lambda, u, t)}{\partial \lambda} \right|\right| ||\delta\lambda|| .$$

The actual parameter uncertainty vector for our hardware setup is $\delta\lambda = (5\%, 5\%, 1\text{ g}, 5\%, 5\%, 0.261\text{ rad}, 5\text{ cm})^T$ that gives an expected landing region represented by a circle of radius $||\delta p(t_f)|| = 1.397$ m. The distance between the experimental landing positions and the theoretical one is characterized by a mean value of $0.57$ m and a standard deviation of $0.23$ m, that is largely contained in the circle.

Therefore, the experiments demonstrates that the proposed model is correct, yet they also reveal a large sensitivity of the open–loop control scheme to intrinsic inaccuracies of the system, which motivates the study of a closed–loop control.

## VI. Conclusion

A novel casting manipulator for reaching objects placed at generic 3D positions was presented. Based on a dynamic model, that is more accurate than the one proposed in previous work, a planning scheme for the trajectory of the end–effector was developed, whose effectiveness was shown during experiments as well as during the first ESA

Lunar Robotics Challenge [9]. The scheme provides a throwing configuration that allows a given target position to be reached. Experiments demonstrated that the proposed model is correct, yet they also revealed a large sensitivity of the open–loop control scheme to intrinsic inaccuracies of the system, which motivates the study of a closed–loop control. In future work, we will in fact investigate the use of the magnetic clutch as an active control to steer the end–effector based on the current target position and end–effector's state.

## VII. Acknowledgments

Authors wish to thank Dr. Riccardo Schiavi, Giorgio Grioli, and the students of the University of Pisa team, Fabrizio Flacco, Gaspare L'Episcopia, Gaetano Lorefice, Federico Puccinelli, Andrea Di Basco, Manolo Garabini, Michael Catanzaro, Fabrizio Vivaldi and Nicola Di Lecce for their contributions to the development of the project as well as the successful result of the competition. This work has been partially supported by the European Commission with Contract IST 045359 (2006) (STREP) "PHRIENDS - Physical Human-Robot Interaction: depENDability and Safety".

## Appendix

The robot's direct kinematics $p = k(q)$ reads

$$\begin{aligned} x &= \tilde{C}_\theta(a_1\tilde{C}_\alpha + \tilde{C}_{\alpha\beta}\tilde{C}_\gamma\rho) + \tilde{S}_\theta(h - \tilde{C}_\beta\tilde{S}_\gamma\rho)\,, \\ y &= a_1\tilde{S}_\alpha + \tilde{C}_\gamma\tilde{S}_{\alpha\beta}\rho\,, \\ z &= -\tilde{S}_\theta(a_1\tilde{C}_\alpha + \tilde{C}_{\alpha\beta}\tilde{C}_\gamma\rho) + \tilde{C}_\theta(h - \tilde{C}_\beta\tilde{S}_\gamma\rho)\,, \end{aligned}$$

where the following standard abbreviations have been used: $\tilde{C}_i = \cos(i)$, $\tilde{S}_i = \sin(i)$, $\tilde{C}_{ij} = \cos(i+j)$, and $\tilde{S}_{ij} = \sin(i+j)$. Its differential kinematics $\dot{p} = J(q)\,\dot{q}$ reads

$$\begin{aligned} \dot{x} &= \tilde{C}_\theta\left(-a_1\tilde{S}_\alpha\dot{\alpha} - \tilde{C}_\gamma\tilde{S}_{\alpha\beta}\rho\left(\dot{\alpha}+\dot{\beta}\right) - \tilde{C}_{\alpha\beta}\tilde{S}_\gamma\rho\dot{\gamma} + \right. \\ &+ \left. \tilde{C}_{\alpha\beta}\tilde{C}_\gamma\dot{\rho}\right) + \tilde{S}_\theta\left(\tilde{S}_\beta\tilde{S}_\gamma\rho\dot{\beta} - \tilde{C}_\beta\tilde{C}_\gamma\rho\dot{\gamma} - \tilde{C}_\beta\tilde{S}_\gamma\dot{\rho}\right)\,, \\ \dot{y} &= a_1\tilde{C}_\alpha\dot{\alpha} + \tilde{C}_{\alpha\beta}\tilde{C}_\gamma\rho\left(\dot{\alpha}+\dot{\beta}\right) - \tilde{S}_{\alpha\beta}\tilde{S}_\gamma\rho\dot{\gamma} + \tilde{C}_\gamma\tilde{S}_{\alpha\beta}\dot{\rho}\,, \\ \dot{z} &= -\tilde{S}_\theta\left(-a_1\tilde{S}_\alpha\dot{\alpha} - \tilde{C}_\gamma\tilde{S}_{\alpha\beta}\rho\left(\dot{\alpha}+\dot{\beta}\right) - \tilde{C}_{\alpha\beta}\tilde{S}_\gamma\rho\dot{\gamma} + \right. \\ &+ \left. \tilde{C}_{\alpha\beta}\tilde{C}_\gamma\dot{\rho}\right) + \tilde{C}_\theta\left(\tilde{S}_\beta\tilde{S}_\gamma\rho\dot{\beta} - \tilde{C}_\beta\tilde{C}_\gamma\rho\dot{\gamma} - \tilde{C}_\beta\tilde{S}_\gamma\dot{\rho}\right)\,. \end{aligned}$$

Finally, its dynamics $\mathrm{B}(q)\,\ddot{q} + h(q,\dot{q}) = \tau$ is characterized by the terms

$$\begin{aligned} b_{11} &= I_\alpha + m\left(a_1^2 + \tilde{C}_\gamma\rho(2a_1\tilde{C}_\beta + \tilde{C}_\gamma\rho)\right)\,, \\ b_{12} &= a_1 m\tilde{C}_\gamma\tilde{S}_\beta\,,\ b_{13} = -a_1 m\tilde{S}_\beta\tilde{S}_\gamma\rho\,, \\ b_{14} &= m\tilde{C}_\gamma\rho(a_1\tilde{C}_\beta + \tilde{C}_\gamma\rho)\,, \\ \\ b_{21} &= a_1 m\tilde{C}_\gamma\tilde{S}_\beta\,,\ b_{22} = \tfrac{I_r}{R_r^2} + m\tilde{C}_\gamma^2 + m\tilde{C}_\beta^2\tilde{S}_\gamma^2\,, \\ b_{23} &= -m\tilde{C}_\gamma\tilde{S}_\beta^2\tilde{S}_\gamma\rho\,,\ b_{24} = -m\tilde{C}_\beta\tilde{S}_\beta\tilde{S}_\gamma^2\rho\,, \\ b_{31} &= -a_1 m\tilde{S}_\beta\tilde{S}_\gamma\rho\,,\ b_{32} = -m\tilde{C}_\gamma\tilde{S}_\beta^2\tilde{S}_\gamma\rho\,, \\ b_{33} &= \tfrac{1}{4}m\left(3 + \tilde{C}_{2\beta} - 2\tilde{C}_{2\gamma}\tilde{S}_\beta^2\right)\rho^2\,, \\ b_{34} &= -m\tilde{C}_\beta\tilde{C}_\gamma\tilde{S}_\beta\tilde{S}_\gamma\rho^2\,, \\ \\ b_{41} &= m\tilde{C}_\gamma\rho(a_1\tilde{C}_\beta + \tilde{C}_\gamma\rho)\,, \\ b_{42} &= -m\tilde{C}_\beta\tilde{S}_\beta\tilde{S}_\gamma^2\rho\,,\ b_{43} = -m\tilde{C}_\beta\tilde{C}_\gamma\tilde{S}_\beta\tilde{S}_\gamma\rho^2\,, \\ b_{44} &= -\tfrac{1}{4}m\left(-3 + \tilde{C}_{2\beta} - 2\tilde{C}_\beta^2\tilde{C}_{2\gamma}\right)\rho^2\,, \end{aligned}$$

$$\begin{aligned} h_\alpha &= m\left(-2a_1\tilde{C}_\beta\left(\dot{\alpha}+\dot{\beta}\right)\left(\tilde{S}_\gamma\rho\dot{\gamma} - \tilde{C}_\gamma\dot{\rho}\right) + \right. \\ &+ 2\tilde{C}_\gamma\rho\left(\dot{\alpha}+\dot{\beta}\right)\left(-\tilde{S}_\gamma\rho\dot{\gamma} + \tilde{C}_\gamma\dot{\rho}\right) + \\ &+ \left. a_1\tilde{S}_\beta\left(-\tilde{C}_\gamma\rho\left(2\dot{\alpha}\dot{\beta} + \dot{\beta}^2 + \dot{\gamma}^2\right) - 2\tilde{S}_\gamma\dot{\gamma}\dot{\rho}\right)\right)\,, \\ h_\rho &= -m\left(\tilde{C}_\gamma(a_1\tilde{C}_\beta + \tilde{C}_\gamma\rho)\dot{\alpha}^2 + 2\tilde{C}_\gamma^2\rho\dot{\alpha}\dot{\beta} + \right. \\ &\rho\left(\left(\tilde{C}_\gamma^2 + \tilde{C}_\beta^2\tilde{S}_\gamma^2\right)\dot{\beta}^2 + 2\tilde{C}_\beta\tilde{C}_\gamma\tilde{S}_\beta\tilde{S}_\gamma\dot{\beta}\dot{\gamma} + \right. \\ &+ \left. \left. \left(\tilde{C}_\gamma^2 + \tilde{C}_\beta^2\tilde{S}_\gamma^2\right)\dot{\gamma}^2\right) + \left(\tilde{S}_{2\beta}\tilde{S}_\gamma^2\dot{\beta} + \tilde{S}_\beta^2\tilde{S}_{2\gamma}\dot{\gamma}\right)\dot{\rho}\right)\,, \\ h_\gamma &= \tfrac{1}{2}m\rho\left(2\tilde{S}_\gamma(a_1\tilde{C}_\beta + \tilde{C}_\gamma\rho)\dot{\alpha}^2 + 2\tilde{S}_{2\gamma}\rho\dot{\alpha}\dot{\beta} + \right. \\ &+ \rho\left(\tilde{S}_\beta^2\tilde{S}_{2\gamma}\dot{\beta}^2 - 2\tilde{C}_\gamma^2\tilde{S}_{2\beta}\dot{\beta}\dot{\gamma} + \tilde{S}_\beta^2\tilde{S}_{2\gamma}\dot{\gamma}^2\right) + \\ &\left. \left(-\tilde{S}_{2\beta}\tilde{S}_{2\gamma}\dot{\beta} + \left(3 + \tilde{C}_{2\beta} - 2\tilde{C}_{2\gamma}\tilde{S}_\beta^2\right)\dot{\gamma}\right)\dot{\rho}\right)\,, \\ h_\beta &= m\rho\left(a_1\tilde{C}_\gamma\tilde{S}_\beta\dot{\alpha}^2 + \tilde{C}_\beta\rho\left(\tilde{S}_\beta\tilde{S}_\gamma^2\dot{\beta}^2 - \tilde{C}_\beta\tilde{S}_{2\gamma}\dot{\beta}\dot{\gamma} + \right.\right. \\ &+ \left.\left. \tilde{S}_\beta\tilde{S}_\gamma^2\dot{\gamma}^2\right) + 2\left(\left(\tilde{C}_\gamma^2 + \tilde{S}_\beta^2\tilde{S}_\gamma^2\right)\dot{\beta} - \tilde{C}_\beta\tilde{C}_\gamma\tilde{S}_\beta\tilde{S}_\gamma\dot{\gamma}\right)\dot{\rho} + \right. \\ &+ \left. 2\tilde{C}_\gamma\dot{\alpha}\left(-\tilde{S}_\gamma\rho\dot{\gamma} + \tilde{C}_\gamma\dot{\rho}\right)\right)\,, \end{aligned}$$

where $I_r$ is the reel inertia and $R_r$ is its radius.

## References

[1] O. Khatib, K. Yokoi, K. Chang, D. Ruspini, R. Holmberg, and A. Casal, "Vehicle/arm coordination and multiple mobile manipulator decentralized cooperation," *Proc. IEEE International Conference on Intelligent Robots and Systems*, 1996.

[2] R. Mamen, "Applying space technologies for human benefit: the canadian experience and global trends," *Canadian Space Agency*, 1986.

[3] H. Mochiyama, E. Shimemura, and H. Kobayashi, "Shape correspondence between a spatial curve and a manipulator with hyper degrees of freedom," *Proc. IEEE International Conference on Intelligent Robots and Systems*, 1998.

[4] N. Takanashi, H. Chose, and J. Burdick, "Simulated and experimental results of dual resolution sensor based planning for hyper redundant manipulators," *Proc. IEEE International Conference on Intelligent Robots and Systems*, 1993.

[5] R. Fisackerly, A. Birk, F. Kirchner, S. Roccella, R. Schiavi, C. Pradalier, C. Rossi, A. Tikanmäki, and C. Brunskill, "The esa lunar robotics challenge: Simulating operations at the lunar south pole," *submitted to Robotics & Automation Magazine*, 2009.

[6] H. Arisumi, K. Yokoi, and K. Komoriya, "Casting manipulation - midair control of gripper by impulsive force," *IEEE Trans. on Robotics*, April, 2008.

[7] A. Fagiolini, H. Arisumi, and A. Bicchi, "Visual-based feedback control of casting manipulation," *Proc. IEEE International Conference on Robotics and Automation*, pp. 2203–2208, 2005.

[8] A. Fagiolini, A. Torelli, and A. Bicchi, "Casting robotic end–effectors to reach far objects in space and planetary missions," *Proc. of 9th ESA Workshop on Advanced Space Technologies for Robotics and Automation*, 2006.

[9] S. Alicino, M. Catalano, F. Bonomo, F. A. W. Belo, G. Grioli, R. Schiavi, A. Fagiolini, and A. Bicchi, "A rough–terrain, casting robot for the esa lunar robotics challenge," *Proc. IEEE International Conference on Intelligent Robots and Systems*, 2009.

[10] T. Suzuki and Y. Ebihara, "Casting control for hyper–flexible manipulation," in *Proc. IEEE International Conference on Robotics and Automation*, 2007, pp. 1369–1374.